



SYMPOSIUM

Visual Acuity in the Flying Snake, *Chrysopelea paradisi*

Shaz A. Zamore ^{*},¹ Nicole Araujo[†] and John J. Socha[‡]

^{*}ATLAS Institute, University of Colorado Boulder, Boulder, CO 80309, USA; [†]Department of Biological Sciences, Virginia Tech, Blacksburg, VA 24061, USA; [‡]Department of Biomedical Engineering and Mechanics, Virginia Tech, Blacksburg, VA 24061, USA

From the symposium “Long Limbless Locomotors: The Mechanics and Biology of Elongate, Limbless Vertebrate Locomotion” presented at the annual meeting of the Society for Integrative and Comparative Biology, January 3–7, 2020 in Austin, Texas.

¹E-mail: sharri.zamore@colorado.edu

Synopsis Visual control during high-speed aerial locomotion requires a visual system adapted for such behaviors. Flying snakes (genus: *Chrysopelea*) are capable of gliding at speeds up to 11 m s^{-1} and perform visual assessments before take-off. Investigating mechanisms of visual control requires a closed-loop experimental system, such as immersive virtual arenas. To characterize vision in the flying snake *Chrysopelea paradisi*, we used digitally reconstructed models of the head to determine a 3D field of vision. We also used optokinetic drum experiments and compared slow-phase optokinetic nystagmus (OKN) speeds to calculate visual acuity, and conducted preliminary experiments to determine whether snakes would respond to closed-loop virtual stimuli. Visual characterization showed that *C. paradisi* likely has a large field of view ($308.5 \pm 6.5^\circ$ azimuthal range), with a considerable binocular region ($33.0 \pm 11.0^\circ$ azimuthal width) that extends overhead. Their visual systems are broadly tuned and motion-sensitive, with mean peak OKN response gains of 0.50 ± 0.11 , seen at $46.06 \pm 11.08 \text{ Hz}$, and a low spatial acuity, with mean peak gain of 0.92 ± 0.41 , seen at 2.89 ± 0.16 cycles per degree (cpd). These characteristics were used to inform settings in an immersive virtual arena, including frame rate, brightness, and stimulus size. In turn, the immersive virtual arena was used to reproduce the optokinetic drum experiments. We elicited OKN in open-loop experiments, with a mean gain of 0.21 ± 0.9 , seen at $0.019 \pm 6 \times 10^{-5}$ cpd and $1.79 \pm 0.01 \text{ Hz}$. In closed-loop experiments, snakes did not exhibit OKN, but held the image fixed, indicating visual stabilization. These results demonstrate that *C. paradisi* responds to visual stimuli in a digital virtual arena. The accessibility and adaptability of the virtual setup make it suitable for future studies of visual control in snakes and other animals in an unconstrained setting.

Introduction

Many flyers rely on complex visual calculations to control the kinematics of their flight. Visual control of locomotion, including flight, is a closed-loop system, where sensory input and motor output influence each other. During locomotion, a visual observer will place their gaze upon objects of interest; visual object detection can then evoke a fixation behavior as a motor output. In order to keep the image stable as the body continues to move, the observer then performs compensatory behaviors of the eye, head, and body. In visual loops, eye and head movements, such as compensatory behaviors during fixation, change subsequent visual input

(Angelaki and Hess 2005), closing the control loop, and allowing visual control of locomotion.

Virtual visual arenas have been increasingly used to explore the role of vision in closed-loop systems across taxa, locomotor types, and ranges of visual ability. These experiments have revealed features of locomotor control, decision-making during navigation, and multisensory integration during locomotion. For example, flying houseflies (*Musca domestica*) will begin to roll in response to rotating visual stimuli (Srinivasan 1977). Fruit flies (*Drosophila melanogaster*) fly toward dark, vertical (tree-like) shapes, while flying away from smaller, circular (predator-like) shapes (Mongeau et al.

2019). Zebrafish larvae use visual feedback to control their prey-capture events (Jouary et al. 2016). Despite the range of taxa that have been studied, there have been few, if any, behavioral investigations using closed-loop experimental apparatuses in reptiles, particularly snakes. This dearth may be partly driven by the possible difficulty of constraining the locomotion of a limbless organism, and the lack of knowledge of their visual systems.

In this study, we characterize the visual system of a limbless reptile, the flying snake (genus *Chrysopelea*), the only snake species known to glide (Socha 2011). As arboreal snakes, *Chrysopelea* live in visually complex 3D environments, scaling trees and crossing branches to hunt, find mates, and escape predators. To glide, a flying snake launches into the air, flattens the body, and laterally undulates. In prior experimental glide trials (Socha 2002, 2006; Socha et al. 2005, 2010; Socha and LaBarbera 2005), flying snakes have been anecdotally observed engaging in visually-mediated behaviors, such as “wagging” the head prior to launch. Although the head wag’s function is unknown, many species, including insects, birds, and mammals, use lateral head oscillation to increase motion parallax (Kral 2003); flying snakes could use similar movements to assess their surroundings visually.

As with other flyers, the visual system of flying snakes must accommodate the particular demands of flight. When gliding, the paradise tree snake (*Chrysopelea paradisi*) attains forward flight speeds up to 11 m s^{-1} (Socha et al. 2005), a locomotor movement that may be as fast as, or faster than, any other species of snake. During glides, in addition to forward translation, the head oscillates both laterally and vertically at 1–2 Hz (Socha et al. 2005), potentially creating a complex, motion-driven visual field. As it glides through the forest, the snake must avoid collisions with trees and foliage, and identify a landing location. Such behaviors are likely to be strongly influenced by vision in gliding animals (e.g., Khandelwal and Hedrick 2020). Furthermore, the paradise tree snake is known to execute visually-mediated behaviors during flight, such as volitional turns. Overall, the locomotor behaviors associated with gliding in flying snakes likely correspond with visual characteristics, as behaviors are known to vary with visual capabilities (Hauzman et al. 2017).

When considering the experimental design of closed-loop visual systems, one must identify key elements of visual characteristics. There is a combination of key features of visual detection that help elicit reflexive behaviors: retinal slip, optic flow, and acuity. Retinal slip is driven by a disparity between

velocities of a retinal image and the eye movement (Abadi and Worfolk 1989). Optic flow arises as a result of relative motion between the observer and the surrounding scene (Borst et al. 2020). Optic flow is dictated by the relationship between the observer and the structure of the visual scene, making it information-rich and valuable for feedback functions. Acuity is the ability to discriminate fine details of a scene, most often examined in spatial, temporal, and spectral dimensions.

Optic flow and retinal slip contribute to more complex visual reflexive behaviors such as optokinetic nystagmus (OKN), a reflexive response that minimizes retinal image velocity and eye velocity disparities. OKN has two distinct parts: (1) **slow phase**: a smooth pursuit that stabilizes the image on the retina, and (2) **fast phase**: a saccadic movement triggered by eye position and velocity (Watanabe et al. 1986; Huang and Neuhaus 2008). These reflexive behaviors, in turn, contribute to voluntary behaviors, including peering behaviors and object avoidance. While visual reflexes, such as OKN, are conserved across a broad diversity of taxa, visual system properties can vary widely (Walls 1962; Huang and Neuhaus 2008), and are not known for many non-model organisms, such as *C. paradisi*. In order to understand visual behaviors in flying snakes, spatial and temporal visual acuity must be measured and associated with characteristic classes of behavior.

The limits of the visual system can be determined from OKN, as the strength of reflexive response varies with visual stimulus difficulty (Koerner and Schiller 1972). Stimulus difficulty can be increased by *increasing* the temporal frequency, as the rate at which patterns pass over the retina approaches the limit of the visual system’s processing rates. Stimulus difficulty can also be increased by *increasing* the spatial frequency, as the spatial density of the waveform peaks becomes smaller than the distances between photoreceptors (Hine et al. 2006; Haug et al. 2010). In this study, we measured slow-phase OKN responses to both physical (“analog”) and digital visual stimuli.

C. paradisi’s combination of visually driven behaviors makes the genus an ideal subject for design of a flexible, immersive virtual visual arena. In this study, we aimed to both identify their visual field and to use their OKN response to characterize the visual system. Based on their ecology, and their predominantly cone-based retina (Simões et al. 2016) which increases retinal spatial resolution, we expected *C. paradisi* to have high temporal and spatial acuities, typical of small, adept flyers, such as budgerigars

(Land 1997; Chaib et al. 2019) or pigeons (Dolan and Fernández-Juricic 2010), but perhaps lower spatial acuity than vision-dependent ambush predators, such as vipers (Brischoux et al. 2010).

In addition to providing a first characterization of the visual behaviors of a flying snake, we also aimed to introduce a new system for studying visual behaviors of unconstrained animals in a virtual reality (VR) arena. Inspired by the growing inclusion of virtual reality arenas in experimental paradigms, we propose a formulaic approach to design of arenas, stimuli, and analysis. Advances in open-source software development platforms and the explosion of the electrical “do it yourself” (DIY) movement make the production of visual, closed-loop arenas both technically and economically feasible for a broad audience of designers.

Methods

Animals

Six flying snakes (*C. paradisi*) in a wild-caught (origin, Malaysia), captive colony were used for the experiments. The animals are housed in a custom-designed facility with temperature and humidity control, which are held between 26°C and 28°C and 50–70% relative humidity, respectively. Animals are housed individually in mesh enclosures (ReptiBreeze, Zoo Med Laboratories, 41 × 41 × 61 cm), outfit with branched polyvinyl chloride (PVC) pipes for climbing, silk leaves, and a translucent hide box. Each enclosure is illuminated with bulbs for heating and ultraviolet light (ReptiZoo, UVB 5) using a 12:12 L:D cycle. Animals are fed frozen/thaw pinky or fuzzy mice once a week in their enclosures, and water is provided *ad libitum*.

Optokinetic experiments

To characterize the visual behaviors and features of the visual system in *C. paradisi*, we measured their spherical field of vision (FOV), low light response threshold, visual acuity (spatial and temporal), and compared frequency and kinematics of visual behaviors. We took three-dimensional (3D) scans of the heads, and, using ray casting, reconstructed the monocular, binocular, and blind regions in their FOV. Then we induced rotational optic flow in an optokinetic drum to determine spatial and temporal acuities, and luminance response. We presented visual stimuli consisting of rotating, vertical square-wave stimuli of different periods, rotated at different velocities. In this setup, animals were free to roam, but were coaxed to stay near the center of the drum, by initially placing each snake in a 6 in (15.24 cm) diameter acrylic petri dish, placed at the center of

the drum (Fig. 1A). The positional time series of the snake’s head was tracked *post hoc*. We classified the observed behaviors and compared kinematics of OKN to determine visual performance.

The optokinetic drum setup was composed of a large, clear acrylic drum (diameter: 45.7 cm; height: 50.8 cm) that rested on a turntable (McMaster Carr, 110 lb. Capacity Spoked Round Turntable) and a raised floor, insulated with high-density foam to minimize motor vibrations (Fig. 1A). We illuminated the drum from overhead using a 50 × 50 cm array of daylight white (6000 K) light-emitting diodes (LEDs) (LE B00HSF65MC), which featured 300 LEDs with 3-cm spacing. The brightness of the array was controlled with a trimpot. On the turntable was a black acrylic mounting plate used for holding the visual stimulus. The visual stimuli were vertical square waves, printed on sheets of white paper (45.7 × 152.4 cm, 300 DPI), mounted onto a cardboard backing for rigidity. Vertical square waves were used to create black and white gratings, with periods of 0.25, 0.34, and 0.51 cm. See [Supplementary Materials](#) for further details of this setup.

To each snake, we presented the visual stimuli at a range of angular velocities. For a given rotational bout, the drum was rotated at a constant velocity, with short (0.5 s) acceleration periods at the beginning and end. The angular velocity of the drum was verified *post hoc* using an optic flow measurement, calculated from a section of the drum captured in the video. Faster angular velocities visibly agitated some snakes, so the duration of the bout was reduced for higher angular velocities. Specifically, slower angular velocities ($<36^\circ \text{ s}^{-1}$) were presented in 3-min bouts in each direction, faster angular velocities ($\geq 36^\circ \text{ s}^{-1}$) were presented in 1-min bouts. The order of direction of the drum rotation (clockwise, counterclockwise) and the order of magnitudes of angular velocities were chosen randomly.

To ensure that behavioral responses did not result from drum vibration, noise, or other stimuli, separate trials were conducted in darkness, to remove the visual input. In these trials, the drum was rotated at either 36 or 48° s⁻¹ under infrared (IR) illumination only (CMVision, IR3, 850 nm). Behavioral responses were identified by the observer and recorded. To measure the luminance threshold, defined as the minimum luminance required to elicit a behavioral response, the drum was first rotated at 36 or 48° s⁻¹ with only IR light. The visible lights were then slowly increased by adjusting the trimpot by hand, and the first instance of behavioral response was noted.

Experiments were carried out at 2000 lux using the range of angular velocities shown in [Table 1](#).

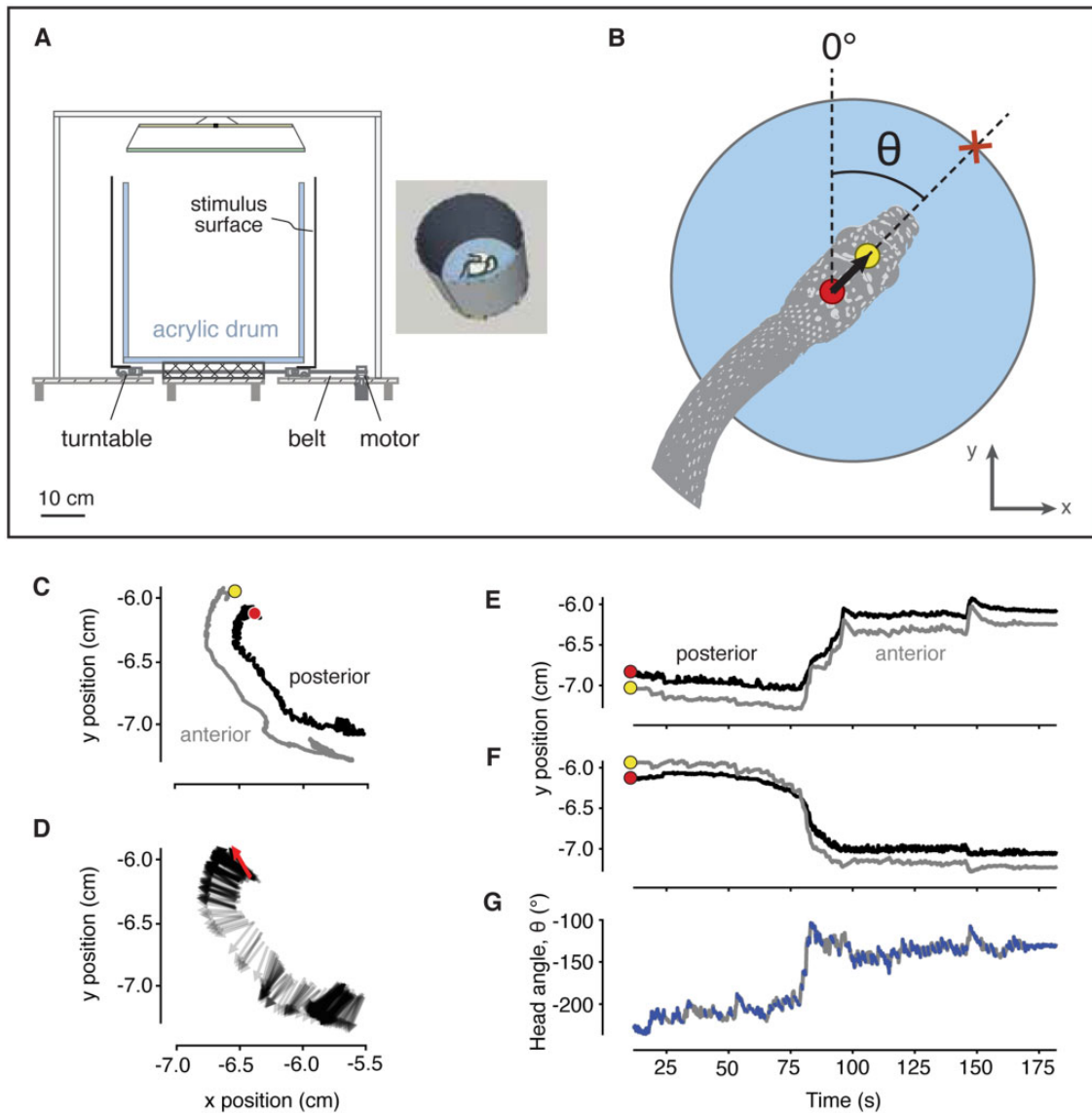


Fig. 1 Optokinetic setup for studying visual behaviors in the snake *C. paradisi*. **(A)** Cutaway and 3D schematic (inset) of optokinetic drum. Snakes were placed in the center of an acrylic drum, in a 6 in (12.54 cm) diameter petri dish (inset, white circle). A vertical square wave stimulus was rotated outside of the drum (inset). The setup was lit from above using a bay of LED lights (upper horizontal band) and a diffuser (lower horizontal band). The acrylic drum was placed on a wooden stand (hatching), which had thick, high-density foam padding (cross-hatch). The visual stimulus (solid black) was attached to a turntable that was rotated by a belt and motor. The entire setup was placed on a floating wooden floor (hatching), supporting by 80/20 beams (gray). The setup was housed in a PVC enclosure (white), which had black felt to block out light (data not shown). **(B)** Head demarcation and vector calculations. Circular dots of acrylic paint were placed on the head for *post hoc* tracking. The inset shows an example of markers on an animal. These markers were used to create a vector (black arrow), from which head angle (θ) was calculated, with the vertical axis of the image set as 0°. This vector was then extrapolated (thin dash) to find the intersecting point on the encompassing drum circumference (red X). The distance from the rostral point (between the eyes) was used to determine viewing distance. **(C)** Time series example of head position in the drum. Points in the red box in the inset are expanded to show the point positions (cm). The large points (red and yellow) indicate initial positions, shown in inset. **(D)** Time series of head vector, with red arrow indicating initial position. To improve visibility, every 10th vector was drawn. Vector arrows are transparent, with darker areas indicating overlap or stillness. **(E–G)** Example positional and head angle time series. Slow-phase OKN is highlighted in blue.

Lighting was measured using a handheld photometer (Pyle PLMT12), placed in the center of the floor of the drum at the approximate height of a snake's head (~ 1 cm).

Light response

A calibration curve was calculated from a series of light values to determine the luminance for light response experiments. Movements of the snakes in the

Table 1 Number of trials for each experimental condition

Square wave period (cm)			
Drum angular velocity (deg s ⁻¹)	0.25 (N animals, n trials)	0.34 (N animals, n trials)	0.51 (N animals, n trials)
3	3, 3	2, 10	4, 4
6	1, 1	1, 4	1, 1
12	0, 0	2, 3	2, 3
18	0, 0	3, 9	4, 6
24	2, 5	2, 2	0, 0
30	1, 1	2, 3	1, 1
36	1, 1	1, 1	2, 2
48	1, 3	2, 2	0, 0
60	1, 1	0, 0	1, 2

This table shows the number of animals and the number of trials used for each permutation of stimulus variables. Animals were presented all stimulus permutations shown, but not all experiments resulted in usable data.

drum were recorded by an infrared-sensitive camera (Raspberry Pi PiNoIR Camera V2) at 60 fps. To allow *post hoc* tracking of movements, two colored marks were placed on the head (Fig. 1B) using acrylic paint prior to experimentation: a yellow marker placed between the supraocular scales, and a red marker along the midline of the parietal scale. Both pigmented paints were applied on top of a white paint mark, which improved the contrast and saturation of the color in the video images. Diameter (4.3 ± 0.8 cm) and distance (10.14 ± 4.9 cm) between markers were measured with digital calipers.

Video analysis

Head movements were digitized using either an open-source Java tracker (Physlet Tracker, <https://physlets.org/tracker/>), or custom Python scripts and OpenCV (<https://github.com/sazamore/Visuomotor-components>) (for data flow diagram, see Supplementary Fig. S1A). Both tracking programs used color filters to isolate the two paint markers. Kalman-filtered Cartesian pixel locations (Fig. 1C and D) of the markers were used to create a head vector, with the tail at the caudal-most position on the head and tip between the eyes (Fig. 1B). This vector was used to characterize the position and orientation of the head, and caudorostral line of sight. From the vector time series, we used custom Python scripting to calculate the viewing distance, defined as the distance to the point on the interior drum that intersects with the extrapolated head vector (Fig. 1B). The viewing distance was used to calculate the spatial density, $f_{spatial}$ in cycles per degree, using:

$$f_{spatial} = \frac{1}{\tan^{-1}\left(\frac{h}{d}\right)} \times \frac{180^\circ}{\pi}, \quad (1)$$

where h is the period of the visual pattern, d is the viewing distance. The inverse tangent is in radians, and converted to degrees. We isolated OKN events using changes in the angle of the vector, defined as head angle, calculated as the angular distance from the horizontal axis of the video (Fig. 1E–G). A peak detector (peakdet, <https://gist.github.com/endolith/250860>) was used to find peaks no closer than 25–30 time steps apart, which was found to work best in isolating the slow-phase OKN response. Spatial frequency was used to derive the temporal frequencies, $f_{temporal}$ which was possible because the rate at which the waves pass over the eye is both a function of the period, distance, and the stimulus' angular velocity. We calculated the temporal frequency using:

$$f_{temporal} = \omega_{drum} \times f_{spatial}, \quad (2)$$

where ω_{drum} is the angular velocity of the drum (deg s⁻¹) and $f_{spatial}$ is calculated using Equation (1), producing a frequency in Hz.

To calculate the average angular velocity of the head, we calculated the mean slope of the slow-phase OKN (Fig. 1E). This velocity was then compared to the drum's angular velocity. To calculate the gain of the OKN response, the angular velocities of the head from a single OKN event were averaged over the entire time series (ω_{head}) and divided by the angular velocity of the drum (ω_{drum}).

$$\text{gain} = \frac{\omega_{\text{head}}}{\omega_{\text{drum}}} \quad (3)$$

Gain values around one indicate strong visual detection, whereas gains below or above one may indicate variances in behavior, often associated with weak or inaccurate visual detection.

3D head scanning

To create 3D images of the head, we laser-scanned the heads of two live, awake snakes (NextEngine, 3D Scanner Ultra HD; captures 268 K pts in⁻² with $\pm 100 \mu\text{m}$ error at 500 DPI). To improve the shape of the modeled spectacle, we first covered the eyes and ventral surface of the head with light blue acrylic paint (Fig. 2A), which also shielded the eye from laser exposure. We used a light blue color, as it produced the most continuous surfaces with the highest spatial resolution for this scanner.

Snakes were held by hand with their heads on the scanner platform and scanned at multiple angles. After scans were complete, the dried paint was peeled off, and any lingering paint was dissolved with diluted isopropyl alcohol (50%). Scans from different angles were stitched together using ScanStudio software. The color differentiation between scales and skin produced spatial noise in the scans (see [Supplementary Materials](#)). The resulting 3D model was then exported to MeshLab and Blender software, and the mesh surface noise was removed, and any holes were interpolated in order to make the mesh continuous. The processed 3D model was then used for inverse perimetry calculations to measure the FOV (Fig. 2B).

Inverse perimetry

To calculate 3D fields of view, we inverted traditional perimetry methods, such that we could map the visual field based on modeled light rays reaching the surface of the spectacle. This method, called inverse perimetry, was used in [Stevens \(2006\)](#). We implemented a virtual inverse perimetry using ray casting, which involves vectors with infinitely large magnitudes that are projected from a given position in 3D space. When calculating FOV, these rays are drawn tangentially to the surface of the eye, and projected outward. Tangent rays are used to measure the maximal angles that can still potentially enter the eye, due to differences in refractory indices of the spectacle and lens.

We used the Unity 3D programming platform to project rays from the vertices of a spherical grid (step sizes: 11° azimuthal, 11.25° elevation) toward

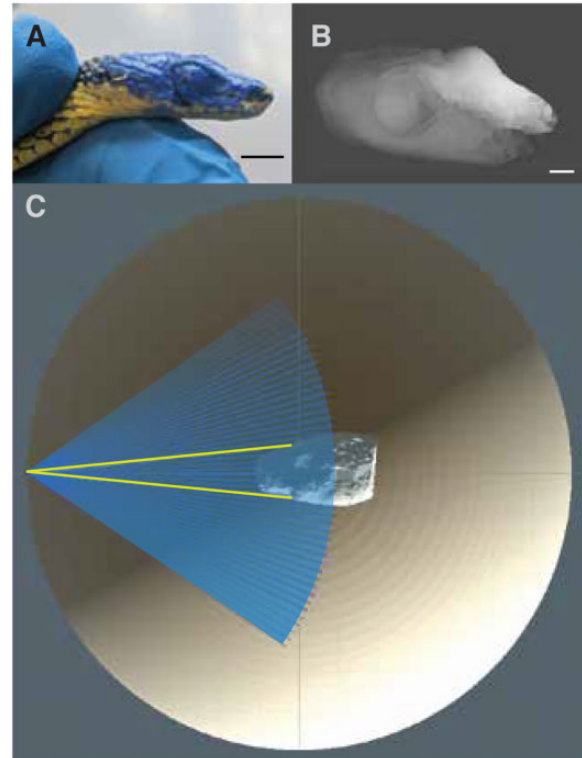


Fig. 2 Methods for determining FOV using 3D scanning. **(A)** Acrylic paint on the head of a male *C. paradisi*. Paint was used to protect the eye and improve scan quality of the spectacle. **(B)** Example reconstruction of the snake heads shown in **(B)** after smoothing. **(C)** Birds-eye view of the reconstructed model scene in Unity 3D. Rays (thin lines) were cast from vertex (origin of rays) in an encompassing sphere. At each point, a spread of rays is cast (thin lines) and eye intersection is determined (thick lines). Vertices were 11° apart in azimuth, and 11.25° in elevation.

the reconstructed digital heads of two snakes, one male and one female (see [Supplementary Materials](#)). At each vertex, a ray was pointed toward the center of the eye and swept $\pm 45^\circ$ in the azimuthal plane (Fig. 2C). This procedure replicates the divergence seen with sunlight, and thus approximates how light would naturally reach the eye. When rays first intercept the eyes, it indicates a putative point of vision; when it first intercepts the head, it indicates a blind region. A sweep of rays at a single vertex may intercept with both eyes, indicating putative binocular regions. Further details are provided in the [Supplementary Material](#).

To identify regions of monocular, binocular, and blindness, we exported the points of interception, and for each point on the grid, we determined if there was one (monocular), two (binocular), or no intercept(s) (blind region). For each resulting monocular and binocular region, we measured the minima, maxima, and ranges of angles in both the azimuth and elevation planes.

OKN Analysis

The slow phase of the detected OKN events (“slow-phase OKN”) were fit with a least-squares linear regression and we discarded any events with slopes that had a low r^2 value ($r^2 \leq 0.85$). We binned the observed values of spatial and temporal frequencies and compared the slow-phase OKN gains for each bin across all test conditions, grouping data by square-wave stimulus period (grating widths) and angular velocity of the drum.

OKN responses across stimuli were non-Gaussian, with binned frequencies repeated across all comparisons. Thus, we used a Friedman test (a non-Gaussian version of analysis of variance (ANOVA)) for our statistical analysis of slow-phase OKN gain. Mean maximum responses were evaluated across the log-transformed dataset and confirmed as statistically representative of the expected mean using a one-sample t -test.

Virtual arena experiments

To test whether *C. paradisi* is responsive to immersive, digital visual stimuli, we built a Cave Automated Virtual Environment-style (CAVE) virtual arena. The arena frame was built with aluminum T-slot framing (80/20, 1010 series) in the form of a raised cube with side lengths of 91.44 cm (Fig. 3A). The walls were fitted with translucent vinyl sheets, onto which images were rear-projected using three high-definition (HD) projectors (VS350 XGA 3LCD; Epson, Japan). To record the position of the snake in the arena, an optical hand-tracking module (Leap Motion Controller) was placed on a custom 3D-printed mount, attached to the ceiling of the arena. The floor of the 80/20 cube was open, allowing placement of a table on which the animals were contained. Atop the table was the same acrylic cylinder used in the optokinetic experiments. The wide-angle cameras within the controller could fully capture the view of the entire acrylic cylinder in which the snake was placed.

Air table

To observe locomotor behaviors within an enclosed small volume, we designed an air table to create a low-friction surface, which enabled the snake to undulate but not easily translate. We estimated the snake’s footprint from the mean cross-sectional width (chord length) when flattened for all points along the snout–vent length (for more detailed information, see [Supplementary Material](#)).

Behavioral tracking

We attached an asymmetrical marker on the head (Fig. 3A) to track the snake in real time. The marker was made of black cardstock and IR-reflective tape. The marker was affixed using removable glue dots. Custom template-matching scripts (Python, OpenCV) were used to determine the position and orientation of the head. The lightweight marker did not obviously impede the snake’s behavior. As with optokinetic drum marker positions, the 3D marker position data were passed through a Kalman filter (pykalman, <https://github.com/pykalman/pykalman>) and then sent to custom Unity 3D software at 30 fps. In frames where the head was not detected, a Kalman estimate was used. Kalman filter parameters were optimized over five iterations, using the built-in Expectation–Maximization algorithm.

We separately placed two individual snakes in the arena and observed their behavioral responses to closed- and open-loop virtual drum rotations. The virtual drum was created with Unity 3D. The virtual optokinetic drum was created to have the same dimensions as the physical one used in previous experiments (Fig. 3B). A single square wave stimulus was used (19.2 cm period), and the drum was rotated at a single velocity (48° s^{-1}). The scene frame rate was 120 Hz, which we confirmed using high-speed videography of the projection. The drum position was logged with the head position data.

In open-loop conditions, the head position was logged and not sent to Unity. In closed-loop conditions, the head position was logged and also sent to Unity. These data were used to update the position of the VR camera, thus changing the projected view in the arena (Fig. 3C) (for script flow diagrams, see [Supplementary Fig. S1B](#)). To deal with the frame rate disparity between devices, a given head position was used for four frames and then updated.

Analysis

As with the optokinetic experiments, we collected the head position data, from which we calculated the head angle time series. We used the head angle time series to detect OKN events in both open- and closed-loop configurations (Fig. 3D and E), and analyzed the behavior with the same procedure as the optokinetic experiments. We also used the reported position of the drum to compare head behaviors to the simulated drum behaviors.

Results

In the optokinetic drum experiments, snakes began to exhibit any behavioral response to rotational

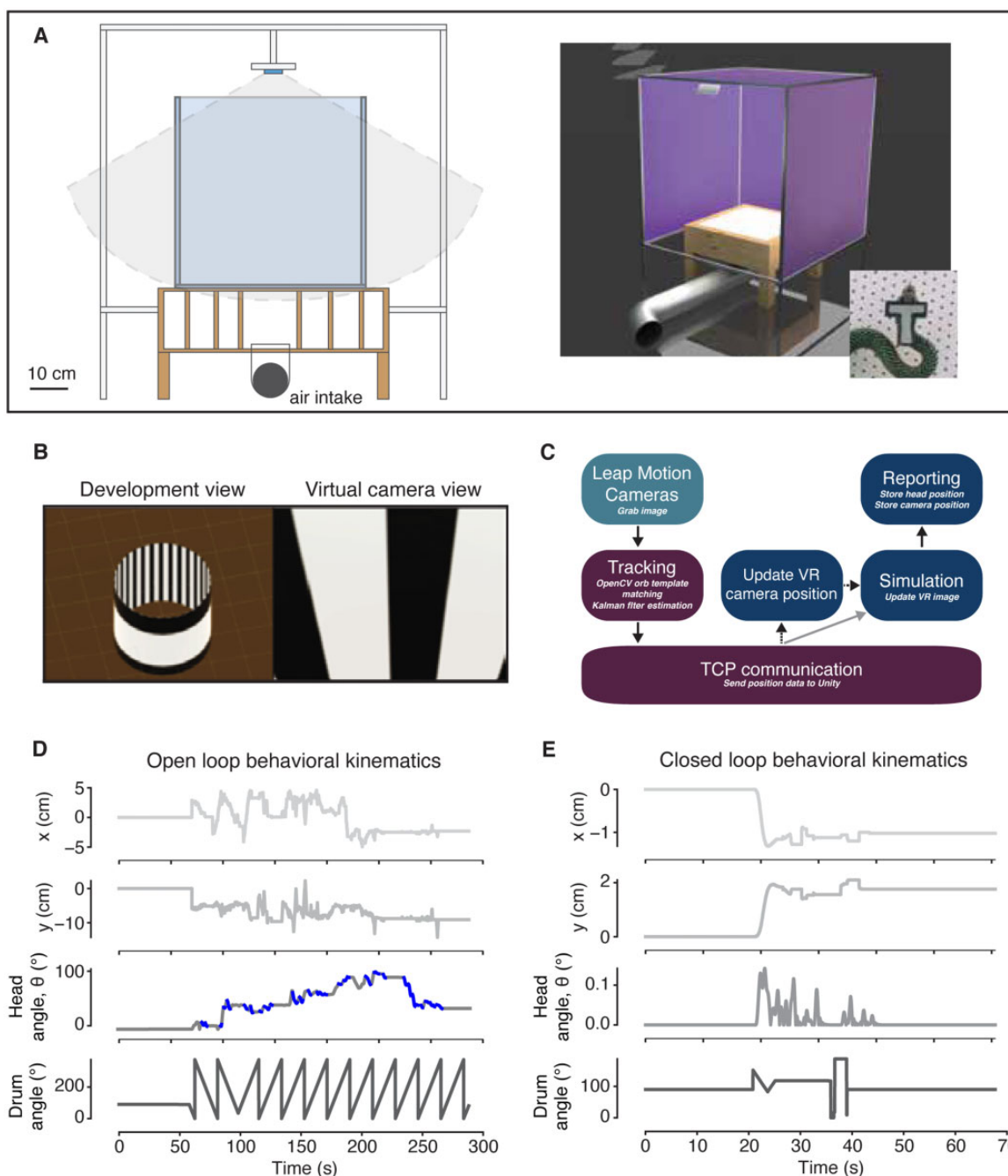


Fig. 3 Immersive virtual visual arena setup for studying visual behaviors in the snake *C. paradisi*. **(A)** Cutaway (left) and 3D schematic (right) of immersive virtual visual arena. A Leap Motion Controller, mounted at the top of the rig, was used to capture snake behaviors (dark blue). LCD projectors (data not shown) were placed outside of the arena and back-projected images onto the walls. An air table was used to create a low-friction surface to snakes during immersive events, with air input coming in from a leaf blower (not shown). Atop the air table, a bottomless acrylic cylinder was placed (solid color). A 3D model of the arena is shown on the right, illustrating three of the four covered walls onto which images were projected. The inset shows the infrared-reflective T-shaped marker (3×4 cm) used to track head position and angle. **(B)** Virtual optokinetic drum, shown in the developer's view (left) and as seen in the experiment, from the virtual camera (right). Virtual drum dimensions were taken from real-world optokinetic drum dimensions. **(C)** Information flow diagram for open- and closed-loop paradigms. For both paradigms (both: black arrows), images from the Leap Motion Controller cameras were passed through Python scripts (Python only: darker color), which used OpenCV Orb template matching to get positions, which were Kalman-filtered to reduce image jitter. The head position data were sent from the Python client via TCP server, hosted in Unity 3D (Unity 3D only: lighter color). In closed-loop experiments (light gray arrow), data were sent through the simulation scripts in Unity 3D (blue) and reported. In closed-loop experiments (dashed arrows), head position data were passed into the Unity 3D scripts and updated the VR camera position. **(D–E)** Example head position time series data from an open-loop and closed-loop trials, respectively. From top to bottom: horizontal (x) and vertical (y) positions (cm), head angle (θ_{head}), with OKN events shown with thicker linewidth, and drum angle (θ_{drum}). The virtual drum was rotated at 48 deg s^{-1} . Horizontal (x) and vertical (y) position time series are shown in cm. Head angle and drum rotation phase time series are shown in degrees. **(D)** The drum rotation was reversed at 100 s. **(E)** The drum rotation phase was shown as perceived by the animal, with a rotation seen between 40 and 50 s, when compensatory behaviors held the virtual drum position fixed. A data artifact can be seen at $t=35$ s; the sign of the head vector, which controls the drum position, flipped, but rendering code prevents any sign changes to be drawn, resulting in a stable image.

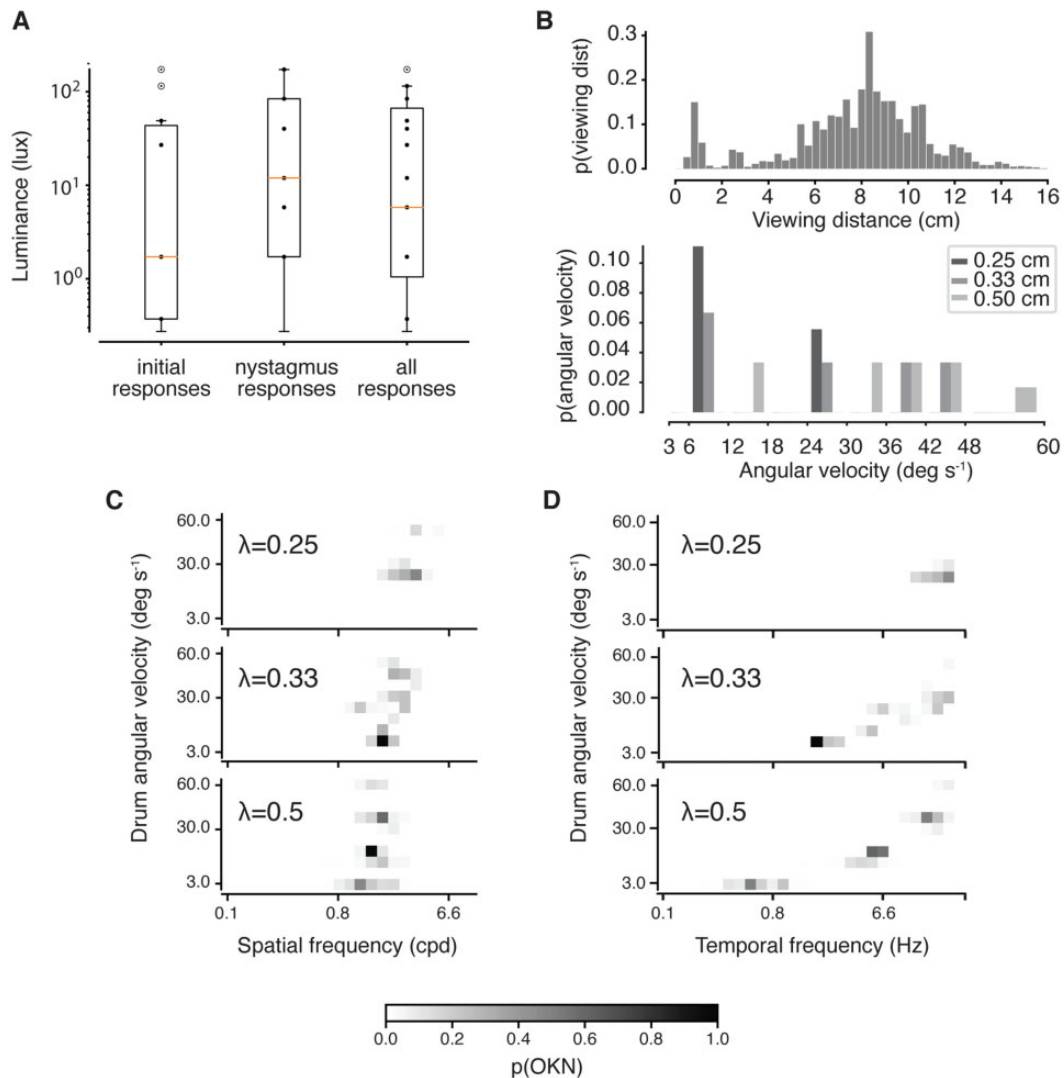


Fig. 4 Ensemble visual and optokinetic responses. **A.** Light response distributions for initial responses, OKN, and combined responses. Response type was characterized by eye, as lighting was slowly brightened in the arena, with the drum rotating. The lighting value at which the response was detected was recorded. There were no significant differences between initial and nystagmus response, nor were there significant differences between individual classes of responses and the total response. **(B)** (Top) Probability distribution function (PDF) of all binned viewing distances seen. Viewing distance PDF for all experimental conditions. The distribution is non-Gaussian. There is a peak occurrence seen at 8.2 cm. (Bottom) PDF for all OKN events. **(C)** *C. paradisi* have low OKN gain values, regardless of stimulus difficulty, with few values at or above an ideal value of one (matching drum angular velocity). **(D)** The 2D probability distribution of OKN gains for all binned spatial frequencies measured. Distributions are shown for each stimulus wavelength ($\lambda = 0.25, 0.33,$ and 0.5 cm), with lighter values indicating lower probabilities. Probability of OKN decreased as angular velocity of the drum increased.

motion at a luminance of 11.6 ± 1.1 lux (mean \pm S.E.M.) (one sample *t*-test, $P=0.03$) (Fig. 4A). We found no significant difference between the mean luminance of initial responses, such as saccades or tracking (7.6 ± 1.3 lux) and luminance when nystagmus responses began (17.8 ± 1.2 lux, one-way *t*-test, $P=0.45$). There was also no difference between initial response and all responses, and nystagmus response and all responses (one-way *t*-test, $P=0.64$, $P=0.67$, respectively). These behaviors were also observed in full-light

behavioral trials, along with a lateral, transitory oscillation of the head (head wagging).

Next, we measured probabilities of viewing distance and OKN occurrence across all test conditions. Because the animal was free to move, the spatial and temporal frequencies were calculated as a function of viewing distance, the distance between the midline of the eyes and the closest point on the drum surface. We found that there was a near-uniform spread of viewing distances, with a distinct peak at 8.2 cm. We also saw a decrease in OKN occurrences as the

drum's angular velocity increased, and this trend was seen across all three stimuli (Fig. 4B).

We found that differences in spatial frequencies (cycles per degree, cpd) at large stimulus wavelengths varied significantly across the drum's angular velocities (Fig. 4C and D). A small stimulus wavelength (0.25 cm) yielded no differences for each binned spatial frequency (Kruskal–Wallis, $P=0.99$) or temporal frequency (Kruskal–Wallis, $P=0.99$) compared across drum angular velocities, but significant differences for each binned spatial frequency was seen with stimulus wavelengths measuring 0.34 and 0.51 cm (Kruskal–Wallis test, $P=0.04$, $P=0.002$, respectively). Looking at responses to temporal frequency changes for all drum angular velocities, at 0.34 cm we saw no differences (Kruskal–Wallis test, $P=0.1$), but the largest wavelength, 0.51 cm, exhibited significant differences across drum angular velocities (Kruskal–Wallis test, $P=0.002$).

We used the optokinetic behaviors to assess the spatial and temporal frequencies that correspond to the snake's peak visual sensitivity and maximal frequencies of response. Across all test conditions, the mean of the maximal OKN gain as a function of spatial frequency was 0.92 ± 0.41 , at 2.89 ± 0.16 cpd (for all values: mean \pm S.E.M.) (Fig. 5A). For temporal frequency, mean of the maximal OKN gain for all trials was 0.50 ± 0.11 , at 46.06 ± 11.08 Hz (Fig. 5B). We found the highest values at which an OKN response to spatial frequency occurred was 4.33 cpd, and for temporal frequency was 84.3 Hz. These values are close to the highest values we presented.

3D FOV

We constructed a putative FOV using 3D digital inverse perimetry with digital models of snake heads (Fig. 6A and B). The calculated azimuthal binocular range is $33.0 \pm 11.0^\circ$, measured with two animals, one male and one female (Fig. 6C and D). The monocular azimuthal range is $154.0 \pm 15.0^\circ$ across all eyes (Table 2). In elevation, the binocular range is $125.5 \pm 26.5^\circ$ (Fig. 6E and F), with a monocular range of $191.0 \pm 30.4^\circ$ across all eyes. The male *C. paradisi* had a considerably smaller head, with similarly sized eyes, which resulted in a larger binocular range with a similar azimuthal overall range (315° in female, 202° in male). No statistical measurements were taken, as statistical power was too low. These data serve as putative measures for further behavioral evaluation of snake vision.

Virtual arena OKN

We observed behaviors of snakes in open- and closed-loop paradigms. These preliminary data

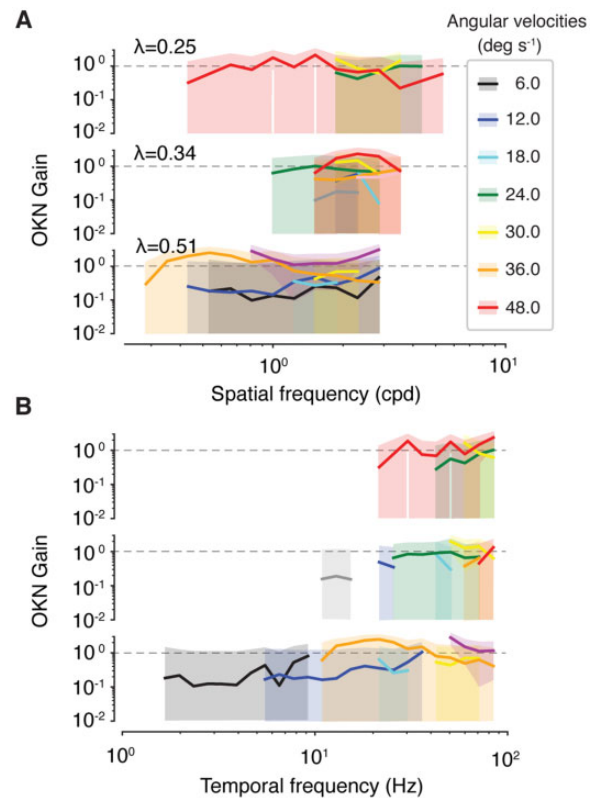


Fig. 5 Characterization of the optokinetic responses. **(A)** Mean OKN gain (solid lines) and standard deviations (translucent color) for all binned spatial frequencies measured, shown for each stimulus wavelength ($\lambda = 0.25, 0.33$, and 0.5 cm). Colors correspond to angular velocity of the drum. Dashed lines indicate a OKN gain of 1, which can indicate peak visual system processing of the stimuli. Standard deviations are skewed from zero value representation on a log–log plot. These graphs illustrate a general trend of improving reflexive response from slower drum angular velocities ($6\text{--}12^\circ \text{ s}^{-1}$), with an increase in performance at higher velocities ($24\text{--}48^\circ \text{ s}^{-1}$). OKN gain has a slight increase over spatial frequencies, with the average of maximal OKN gain being 0.92 ± 0.41 (mean \pm S.E.M.). This narrow spread of OKN gains across spatial frequencies suggests a broad range of peak sensitivities. **(B)** Mean OKN gain and standard deviations for all binned temporal frequencies measured; same color organization as **(A)**. These graphs illustrate a steady increase in OKN gain as temporal frequencies increase, seen in all stimulus wavelengths. Whereas the average of the maximal OKN gain was 0.50 ± 0.11 , higher angular velocities (24° s^{-1}) have an OKN gain closer to one, suggesting a range of peak sensitivities in the higher range of our tested temporal frequencies.

represent the potential viability of using limbless animals locomoting in closed-loop visual arenas.

For the open-loop behaviors, we observed 30 OKN events, which occurred within a small range of spatial and temporal frequencies. Thus, we can compare the observed behaviors within the optokinetic drum behaviors, but not virtual arena behaviors. In our test trials, we measured an OKN gain of 0.21 ± 0.9 for spatial frequency values of

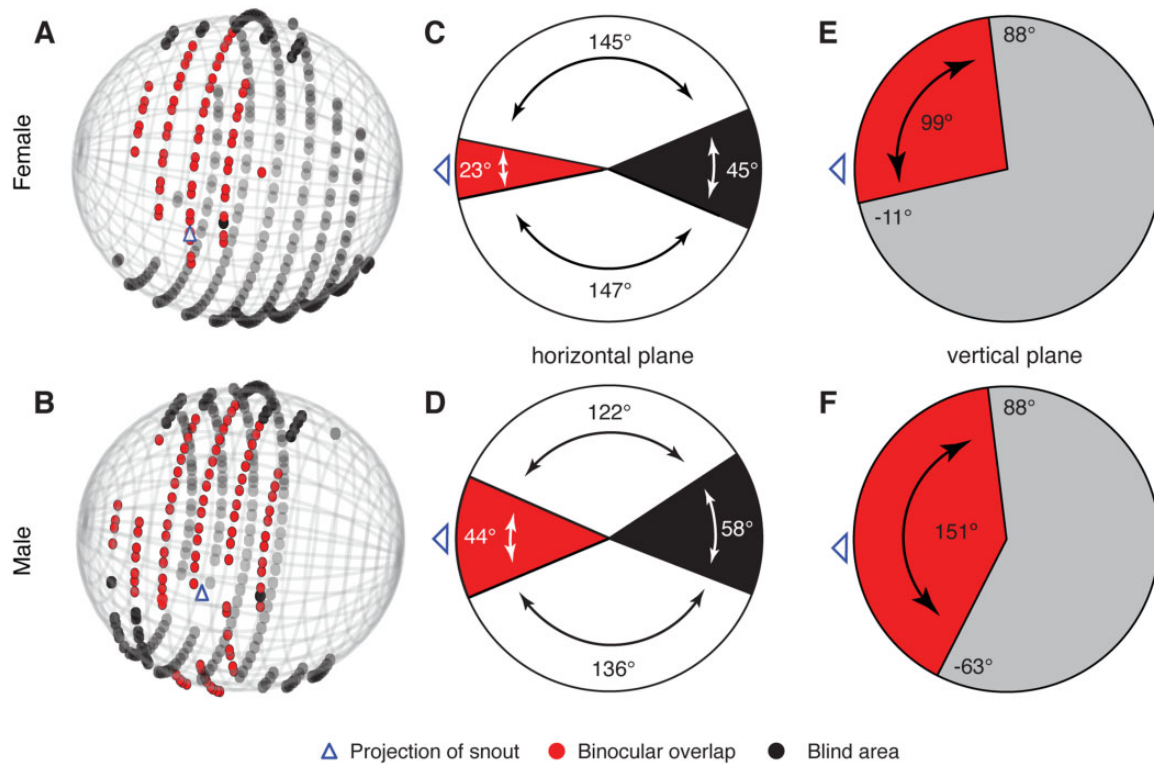


Fig. 6. Putative visual FOV of the flying snake *C. paradisi*. 3D reconstruction of orthographic projection of visual field for (A) female and (B) male snakes. For all images, lighter coloration (red) indicates binocular regions, and black represent blind regions. Points at a greater depth are more translucent. Location of the snout projection is shown with blue triangles in the center of the world view, with the snake’s eyes at the center of the sphere. (C and D) Midline projection of the horizontal (azimuthal) plane showing the visual field. White indicates monocular range, not including the binocular region. (E and F) Projection of the vertical (elevation) plane of the binocular region. Negative values are below horizontal, positive values are above horizontal. Light gray represents the remainder of the visual field.

Table 2 Results of 3D FOV measurements

Azimuth		Elevation						
Animal		Min	Max	Range	Min	Max	Range	
89 (M)	Left	-22.0	122.0	144.0	Left	-101.0	114.0	215.0
	Right	22.0	-158.0	180.0	Right	-113.0	114.0	227.0
	Binocular	-22.0	22.0	44.0	Binocular	-63.0	88.0	152.0
81 (F)	Left	-11.0	169.0	147.0	Left	-41.0	116.0	157.0
	Right	11.0	-156.0	145.0	Right	-55.0	110.0	165.0
	Binocular	-11.0	11.0	22.0	Binocular	-11.0	88.0	99.0

The values shown represent the azimuthal and elevation dimensions for the projected FOV. Ranges of angle for each eye and binocularity are listed. For the azimuthal plane, positive values represent the right-hand side of the head midline; negative values represent the left-hand side. Monocular ranges include the region of binocular overlap. For the elevation plane, positive values are above the head midline, negative values are below the midline. The midline of the head is at 0° for both azimuth and elevation. The male’s (89) head and eye are smaller than that of the female (81).

$0.019 \pm 6 \times 10^{-5}$ cpd and temporal frequency values of 1.79 ± 0.01 Hz (see [Supplementary Material](#)).

For closed-loop behaviors, we observed no OKN events in the head angle of the snake. Thus, direct comparison to optokinetic drum

data could not be conducted. Instead, we measured the angular velocity of the virtual drum as a response to the snake movement and found that drum rotation was slowed and held steady ($0.57 \pm 0.15^\circ \text{ s}^{-1}$).

Discussion

These experiments present the first behavioral assessment of visual acuity in the flying snake *C. paradisi* using strength of OKN response, a modified method of inverse perimetry, and a proof of-concept demonstration that virtual reality is effective for exploring visually-mediated snake behaviors. With little visual acuity data snakes, this work provides valuable insight into visual control of locomotion-related behaviors, as well as helping to set the foundations for comparative visual work across snake species. We found our data to coincide with trends seen in other taxa, in that slow-phase OKN gain would decrease with processing difficulty (i.e., high temporal and spatial frequencies; Schweigart and Hoffmann 1992; Gioanni et al. 1993; Haug et al. 2010; Distler and Hoffmann 2011). We found the peak frequency of response occurred at slow angular velocities of the drum and larger periods of the stimulus (Fig. 4B), and peak acuity sensitivities around 2.89 ± 0.49 cpd and 46.06 ± 11.08 Hz at 2000 lux (see Supplemental Material). The snakes exhibited a broad range of slowly changing OKN gain, suggesting a highly adaptable visual system. Although head OKN became less frequent at higher temporal frequencies, we did not see an expected drop in gain. This result may be due to corollary discharge, where the visual system anticipates an increase in visual difficulty (Koerner and Schiller 1972). We also observed lateral oscillatory translations (head wagging) with more visually challenging stimuli. This behavior may be an evoked response, inducing head movements similar to those seen during gliding.

Our method of virtual ray casting was used to conduct inverse perimetry to identify FOV. These data indicate that flying snakes have a wide-field azimuthal view ($297.5 \pm 5.5^\circ$) (Fig. 6A, B), with an azimuthal binocular range of $23.5 \pm 0.5^\circ$. Our results suggest that the flying snake *C. paradisi* is well-equipped for high-speed, motion-based visual processing, which might occur while gliding, fleeing predators, or chasing or striking prey. The binocular FOV in *C. paradisi* has a large range in elevation that includes overhead angles, with the upper limit of the binocular region nearly directly above the head (88° above horizontal). This range may help explain their sensitivity to overhead movement. Under experimental conditions of glide trials in the field, flying snakes have been observed to visually track objects moving in the sky, including birds and airplanes (Socha and Sidor 2005), suggesting that this genus has a large, motion-sensitive visual field, a feature that could be related to predation pressures from birds of prey.

Furthermore, *Chrysopelea* is a sister taxon to *Dendrelaphis*, *Ahaetulla*, and *Dryophiops* (Figuera et al. 2016). As diurnal, arboreal snakes, these species may share visual adaptations such as large binocular regions and foveae (Simões et al. 2016), as all species in *Chrysopela* and sister taxa live in a complex 3D environment.

Finally, we found that *C. paradisi* exhibits a low-level light response, with mean visual responses occurring at an illuminance of ~ 11 lux. These illuminance levels are equivalent to twilight (https://www.engineeringtoolbox.com/light-level-rooms-d_708.html). Such low-light sensitivity may aid in visual performance in dark areas such as tree cavities or low-light forest conditions, suggesting that specific aspects of the visual system may be adapted to their specific behavioral and ecological niche (Hauzman et al. 2017).

To begin to elucidate the behavioral value of these visual system features, we presented the snakes with an immersive digital scene, in both open- and closed-loop paradigms. In this novel set-up, we had attempted to constrain locomotion by using an air table that reduced frictional forces underneath the snake, limiting translation (Fig. 3A). Based on our visual observations during trials, frictional forces might have been generated when a snake articulated its keeled ventral scales along the holes of the surface of the table (e.g., Jayne et al. 2015).

Virtual arena evaluation, in comparison to analog experiments

Our data represent initial developments that demonstrate the viability of studying snakes in closed- and open-loop virtual arena experiments. With the virtual arena, we aimed to compare similar stimuli to determine if the digital stimulus evoked similar behavioral responses. Despite differences, we successfully elicited OKN in both experimental setups. When directly compared to the analog OKN PDF seen at 48° s^{-1} , these data are in agreement.

In the virtual arena, we saw repeated OKN events across a small range of frequencies. This small acuity range may be caused by inadvertently producing a far-field stimulus. Though we scaled our digital scene to match the optokinetic drum, projection geometry may have affected perceived drum height and diameter, leading to a slightly varied behavioral output. However, even with these potential differences, the mean virtual arena OKN gain occurred within the distribution of optokinetic drum OKN gain values, and the OKN frequency within the distribution of optokinetic drum frequencies. For these reasons, we

consider the VR behaviors demonstrative, but preliminary.

In both systems and for most paradigms, we saw low OKN gain. Low gain can be caused by environments with low contrast sensitivity (Tappeiner et al. 2012). However, we presented stimuli three orders of magnitude above the initial light response, so we do not consider this response to be a consequence of low-light conditions. The head OKN may capture only part of the entire OKN response, with much of the gain described by the unobserved eye movements. OKN gain is driven by retinal slip velocity and contrast—the larger the disparity between head and vision movement, the stronger the OKN response (Maioli and Precht 1984). Our stimuli may only induce a small retinal slip velocity, given the size of the eye (~5 mm) relative to the size of our stimulus wavelength (~7 mm). Our setups may have elicited low retinal slip velocities, which may not evoke the recruitment of head compensatory behaviors. Thus, we would observe fewer head OKN events, as the eye alone can perform gaze stabilization behaviors (Schweigart and Hoffmann 1992).

We also presented the snakes with a closed-loop, rotating virtual drum, and observed a near constant response after an initial adjustment (Fig. 3E). This response indicates that the snake utilized a smooth pursuit that matches the rotation of the drum that resulted in a steady image in the arena. A similar behavior has been seen in hawkmoths (*Manduca sexta*) and fruit flies (*Drosophila spp.*) in visual arenas with similar, rotational experimental paradigms (Hinterwirth and Daniel 2010; Mongeau et al. 2019). This finding also exemplifies the potential of using closed-loop setups to explore known visual behaviors, as the visual function (here, OKN) was confirmed.

For both analog and digital experimental conditions, the animals were free to move, but were encouraged to stay in a central location by initially placing them in a large petri dish. This method likely limited the range of viewing distances. The peak viewing distance was 8.3 cm across all trials (Fig. 4B), which is approximately the distance from the drum circumference to the edge of the petri dish (8.02 cm) (Fig. 1A). Finally, the virtual arena we developed uses all custom-built, open-source software, making it accessible to a wide audience. (Scripts and software developments can be found at <https://github.com/sazamore/VizSciVR>.) The design can be adapted to be used with monitors as well as projection, and modifications to the presented scenes can be made by the user. Virtual scenes were developed to replicate canonical behavioral paradigms including

optokinetic drum and optic flow fields. Combined with design for an air table, we have created, and preliminarily tested, an effective setup for use in evaluating visual behaviors in snakes.

Acknowledgments

We thank Henry Astley for inviting us to participate in this symposium, and for support from Ulrike Müller and Suzanne Miller. We would also like to thank Lauren Bochicchio and Alok Baral for assistance with optokinetic drum experiments, Michelle Graham for suggesting the air table design, Michael Collver for the air table construction, Wallace Lages for help with the LEAP sensor and virtual arena design, Talia Weiss for technical advisement, Yakir Gagnon for help with FOV analysis, and Sönke Johnsen and Bruce Jayne for helpful discussion (Bruce, a box of Milk Duds is on the way). We also thank two anonymous reviewers for their helpful feedback to improve the manuscript.

Funding

This research was supported by an NSF Postdoctoral Research Fellowship (1402558) to S.A.Z. and an NSF CAREER award (1351322) to J.J.S. .

Author Contributions

S. A. Z., and J. J. S. conceived of the project. S. A. Z. designed and conducted experiments and analyzed the data. N. A. and S. A. Z. collected the head scan data. N. A. formulated the head scan stitching procedure. S. A. Z., N.A., and J. J. S. assisted in writing and editing the manuscript. S. A. Z and J. J. S. revised the paper.

Supplementary data

Supplementary data available at *ICB* online.

References

- Abadi R, Worfolk R. 1989. Retinal slip velocities in congenital nystagmus. *Vision Res* 29:195–205.
- Angelaki DE, Hess BJ. 2005. Self-motion-induced eye movements: effects on visual acuity and navigation. *Nat Rev Neurosci* 6:966–76.
- Borst A, Haag J, Mauss AS. 2020. How fly neurons compute the direction of visual motion. *J Compar Physiol A* 206:109–16.
- Brischoux F, Pizzatto L, Shine R. 2010. Insights into the adaptive significance of vertical pupil shape in snakes. *J Evol Biol* 23:1878–85.
- Chaib S, Ljungholm M, Lind O, Kelber A. 2019. Single target acuity is not higher than grating acuity in a bird, the budgerigar. *Vision Res* 160:37–42.

- Distler C, Hoffmann KP. 2011. Visual pathway for the optokinetic reflex in infant macaque monkeys. *J Neurosci* 31:17659–68.
- Dolan T, Fernández-Juricic E. 2010. Retinal ganglion cell topography of five species of ground-foraging birds. *Brain Behav Evol* 75:111–21.
- Figueroa A, McKelvy AD, Grismer LL, Bell CD, Lailvaux SP. 2016. A species-level phylogeny of extant snakes with description of a new colubrid subfamily and genus. *PLoS One* 11:e0161070.
- Gioanni H, Bennis M, Sansonetti A. 1993. Visual and vestibular reflexes that stabilize gaze in the chameleon. *Vis Neurosci* 10:947–56.
- Haug MF, Biehlaier O, Mueller KP, Neuhauss SC. 2010. Visual acuity in larval zebrafish: behavior and histology. *Front Zool* 7:8.
- Hauzman E, Bonci D, Suárez-Villota E, Neitz M, Ventura D. 2017. Daily activity patterns influence retinal morphology, signatures of selection, and spectral tuning of opsin genes in colubrid snakes. *BMC Evol Biol* 17:249.
- Hine TJ, Wallis G, Wood JM, Stavrou EP. 2006. Reflexive optokinetic nystagmus in younger and older observers under photopic and mesopic viewing conditions. *Invest Ophthalmol Vis Sci* 47:5288–94.
- Hinterwirth AJ, Daniel TL. 2010. Antennae in the hawkmoth *Manduca sexta* (Lepidoptera, Sphingidae) mediate abdominal flexion in response to mechanical stimuli. *J Compar Physiol A* 196:947–56.
- Huang YY, Neuhauss S. 2008. The optokinetic response in zebrafish and its applications. *Front Biosci* 13:1899–916.
- Jayne BC, Newman SJ, Zentkovich MM, Berns HM. 2015. Why arboreal snakes should not be cylindrical: body shape, incline and surface roughness have interactive effects on locomotion. *J Exp Biol* 218:3978–86.
- Jouary A, Haudrechy M, Candelier R, Sumbre G. 2016. A 2D virtual reality system for visual goal-driven navigation in zebrafish larvae. *Sci Rep* 6:1–13.
- Khandelwal PC, Hedrick TL. 2020. How biomechanics, path planning and sensing enable gliding flight in a natural environment. *Proc Royal Soc B* 287:20192888.
- Koerner F, Schiller PH. 1972. The optokinetic response under open and closed loop conditions in the monkey. *Exp Brain Res* 14:318–30.
- Kral K. 2003. Behavioural–analytical studies of the role of head movements in depth perception in insects, birds and mammals. *Behav Proc* 64:1–12.
- Land MF. 1997. Visual acuity in insects. *Ann Rev Entomol* 42:147–77.
- Maioli C, Precht W. 1984. The horizontal optokinetic nystagmus in the cat. *Exp Brain Res* 55:494–506.
- Mongeau JM, Cheng KY, Aptekar J, Frye MA. 2019. Visuomotor strategies for object approach and aversion in *Drosophila melanogaster*. *J Exp Biol* 222:jeb193730.
- Schweigart G, Hoffmann KP. 1992. Pretectal jerk neuron activity during saccadic eye movements and visual stimulations in the cat. *Exp Brain Res* 91:273–83.
- Simões BF, Sampaio FL, Douglas RH, Kodandaramaiah U, Casewell NR, Harrison RA, Hart NS, Partridge JC, Hunt DM, Gower DJ. 2016. Visual pigments, ocular filters and the evolution of snake vision. *Mol Biol Evol* 33:2483–95.
- Socha JJ. 2002. Gliding flight in the paradise tree snake. *Nature* 418:603–4.
- Socha JJ. 2006. Becoming airborne without legs: the kinematics of take-off in a flying snake, *Chrysopelea paradisi*. *J Exp Biol* 209:3358–69.
- Socha JJ. 2011. Gliding flight in *Chrysopelea*: turning a snake into a wing. *Integr Comp Biol* 51:969–82.
- Socha JJ, LaBarbera M. 2005. Effects of size and behavior on aerial performance of two species of flying snakes (*Chrysopelea*). *J Exp Biol* 208:1835–47.
- Socha JJ, Miklasz K, Jafari F, Vlachos PP. 2010. Non-equilibrium trajectory dynamics and the kinematics of gliding in a flying snake. *Bioinspiration Biomim* 5:045002.
- Socha JJ, O’Dempsey T, LaBarbera M. 2005. A 3-D kinematic analysis of gliding in a flying snake, *Chrysopelea paradisi*. *J Exp Biol* 208:1817–33.
- Socha JJ, Sidor CA. 2005. *Chrysopelea ornata*, *C. paradisi* (flying snakes). *Behav Herpetol Rev* 36:190–1.
- Srinivasan MV. 1977. A visually-evoked roll response in the housefly. *J Compar Physiol* 119:1–14.
- Stevens KA. 2006. Binocular vision in theropod dinosaurs. *J Vertebr Paleontol* 26:321–30.
- Tappeiner C, Gerber S, Enzmann V, Balmer J, Jazwinska A, Tschopp M. 2012. Visual acuity and contrast sensitivity of adult zebrafish. *Front Zool* 9:10.
- Walls G. 1962. The evolutionary history of eye movements. *Vision Res* 2:69–80.
- Watanabe Y, Ohashi N, Ohmura A, Itoh M, Mizukoshi K. 1986. Gain of slow-phase velocity of optokinetic nystagmus. *Auris Nasus Larynx* 13:S63–S68.